Oxidation of manganese in an ancient aquifer, Kimberley formation, Gale crater, Mars

Nina L. Lanza[1*], Roger C. Wiens[1], Raymond E. Arvidson[2], Benton C. Clark[3], Woodward W. Fischer[4], Ralf Gellert[5], John P. Grotzinger[4], Joel A. Hurowitz[6], Scott M. McLennan[6], Richard V. Morris[7], Melissa S. Rice[8], James F. Bell III[9], Jeffrey A. Berger[10], Diana L. Blaney[11], Nathan T. Bridges[12], Fred Calef III[11], John L. Campbell[5], Samuel M. Clegg[1], Agnes Cousin[13], Kenneth S. Edgett[14], Cécile Fabre[15], Martin R. Fisk[16], Olivier Forni[13], Jens Frydenvang[17], Keian R. Hardy[18], Craig Hardgrove[9], Jeffrey R. Johnson[12], Jeremie Lasue[13], Stéphane Le Mouélic[19], Michael C. Malin[14], Nicolas Mangold[19], Javier Martìn-Torres[20, 21], Sylvestre Maurice[13], Marie J. McBride[22], Douglas W. Ming[7], Horton E. Newsom[23], Ann M. Ollila[1], Violaine Sautter[24], Susanne Schröder[13], Lucy M. Thompson[25], Allan H. Treiman[26], Scott VanBommel[5], David T. Vaniman[27], Marìa-Paz Zorzano[20, 28].

[1]Los Alamos National Laboratory, Los Alamos, NM, U.S.A.
[2]Washington University in Saint Louis, St. Louis, MO, U.S.A.
[3]Space Science Institute, Boulder, CO, U.S.A.
[4]California Institute of Technology, Pasadena, CA, U.S.A.
[5]University of Guelph, Guelph, Ontario, N1G 2W1, Canada.
[6]Stony Brook University, Stony Brook, NY, U.S.A.
[7]NASA Johnson Space Center, Houston, TX, U.S.A.
[8]Western Washington University, Bellingham, WA, U.S.A.
[9]Arizona State University, Tempe, AZ.
[10]University of Western Ontario, London, Ontario, N6A 5B7, Canada.
[11]Jet Propulsion Laboratory, Pasadena, CA, U.S.A.
[12]APL, Johns Hopkins University, Laurel, MD, U.S.A.
[13]Institut de Recherche en Astrophysique et Planétologie (IRAP), Toulouse, France.
[14]Malin Space Science Systems, San Diego, CA, U.S.A.
[15]Université de Lorraine, Nancy, France.
[16]Oregon State University, Corvallis, OR, U.S.A.
[17]Niels Bohr Institute, University of Copenhagen, Copenhagen, Denmark.
[18]U.S. Naval Academy, Annapolis, MD, U.S.A.
[19] LPGNantes, CNRS UMR 6112, Université de Nantes, Nantes, France.
[20]Luleå University of Technology, Kiruna, Sweden.[21]Instituto Andaluz de Ciencias de la Tierra (CSIC-UGR), Granada, Spain.
[22]Purdue University, West Lafayette, IN, U.S.A.
[23]University of New Mexico, Albuquerque, NM, U.S.A.
[24]IMPMC, Muséum d'Histoire Naturelle, 75005 Paris, France.
[25]Univeristy of New Brunswick, New Brunswick, Canada.
[26]Lunar and Planetary Institute, Houston, TX, U.S.A.
[27]Planetary Science Institute, Tucson, AZ, U.S.A.
[28]ICentro de Astrobiologia (INTA-CSIC), Madrid, Spain.

Corresponding author: Nina Lanza (nlanza@lanl.gov)

Key Points:

- Mn-rich fracture fills discovered on Mars
- Chemistry and context indicate Mn-oxides
- Past Mars may have had molecular oxygen

This article has been accepted for publication and undergone full peer review but has not been through the copyediting, typesetting, pagination and proofreading process which may lead to differences between this version and the Version of Record. Please cite this article as doi: 10.1002/GRL.54629

Abstract

The Curiosity rover observed high-Mn abundances (>25 wt% MnO) in fracture-filling materials that crosscut sandstones in the Kimberley region of Gale crater, Mars. The correlation between Mn and trace metal abundances plus the lack of correlation between Mn and elements such as S, Cl, and C, reveals that these deposits are Mn-oxides rather than evaporites or other salts. On Earth, environments that concentrate Mn and deposit Mn minerals require water and highly oxidizing conditions, hence these findings suggest that similar processes occurred on Mars. Based on the strong association between Mn-oxide deposition and evolving atmospheric dioxygen levels on Earth, the presence of these Mn-phases on Mars suggests that there was more abundant molecular oxygen within the atmosphere and some groundwaters of ancient Mars than in the present day.

1. Introduction

High Mn concentrations provide unique indicators of water-rich environments and their redox states. Manganese(II) substitutes for Fe(II) in a wide range of igneous minerals, and silicate weathering provides a substantial source of $Mn^{2+}_{(aq)}$ in surface and ground waters. To precipitate and concentrate Mn in rocks and sediments, high-potential oxidants (much higher than that needed for Fe or S) are required to oxidize Mn to insoluble, high-valence oxides. Consequently, Mn-rich rocks on Earth closely track the rise of atmospheric oxygen [*Johnson et al*., 2013; *Maynard*, 2010; *Hazen et al.*, 2008; *Kirschvink et al.*, 2000; *Johnson et al.*, 2016].

Given the association between Mn-rich rocks and the redox state of surface environments, observations of anomalous Mn enrichments on Mars raise similar questions about redox history, solubility and aqueous transport, and availability as a metabolic substrate. In the first 360 sols of the Mars Science Laboratory (MSL) Curiosity rover mission, ~3% of rock targets analyzed by the ChemCam instrument suite were found to contain Mn abundances greater than ~3 times the value expected for martian basalts [*Lanza et al.*, 2014] based on previous in situ measurements [*Taylor and McLennan*, 2009]. However, the phase, source, and timing of deposition of these Mn enrichments were insufficiently constrained by the geological context, leaving basic questions about the phases and processes responsible for the Mn mineralization. Since this first report, we have made observations of new Mn-rich sedimentary rocks in the Kimberley region along with the stronger geological context needed to constrain the origin of these materials (Fig. 1). Our results show that at least some of the high Mn phases present in Gale Crater occur as Mn-oxides filling veins that crosscut sandstones, requiring post-depositional precipitation as highly oxidizing fluids moved through the fractured strata after their deposition and lithification.

2. Kimberley field site geological context

Curiosity spent sols 576-632 analyzing outcrops of sandstone, siltstone, and conglomerate in a region of Aeolis Palus informally named Kimberley formation (Fig. 1). The exposed strata contained three informal members: the lowermost "Square Top" member, an overlying "Dillinger" member, and the uppermost "Mt. Remarkable" member [*Grotzinger et al.*, 2015; *Le Deit et al.*, 2016]. Following reconnaissance, the Dillinger member became the target for drilling at a site named Windjana (Fig. 1b, 1c). The drilled outcrop exposed sandstones formed by centimeter-scale stratification organized into bedsets 10-20 cm thick that display low angle, planar to trough crossbedding. Examination with the Mars Hand Lens Imager

(MAHLI) revealed medium- to fine-grained sediments [*Stack et al.*, 2016] (e.g. Fig. 2d, Fig. 3b). A range of sediment transport directions, reconstructed from crossbed dip directions, suggests paleoflow hydraulics with a primarily southwesterly flow in an ancient fluvial (or possibly mixed fluvial-aeolian) system [*Grotzinger et al.*, 2015]. Results from the CheMin X-ray diffraction instrument at Dillinger on the Windjana target observed a mixture of minerals consistent with basalt, trachyte, and shergottite compositions, with little evidence for significant aqueous alteration [*Treiman et al.*, 2016].

A notable feature of the Dillinger member is crosscutting "fins" that are more resistant than the surrounding rock (Fig. 1b, 1c, 1d, 1e). These features are interpreted as thin, mineral-filled fractures (veins) exposed by differential aeolian abrasion of the surrounding country rock. The veins typically run parallel to bedding planes, perhaps exploiting them as zones of weakness. We infer that this fracture network created the porosity and permeability that allowed subsurface fluids to move preferentially along these paths of higher hydraulic conductivity. Mineral precipitation—including Mn-rich phases—occurred during fluid flow, and eventually occluded much or all of the fracture porosity.

Kimberley rocks differ in composition from previous study areas in Gale such as the Sheepbed member in Yellowknife Bay [*McLennan et al.*, 2014]. The rocks at Kimberley are enriched in K [*Le Deit et al.*, 2016], matching the substantial fraction of K-feldspar observed by X-ray diffraction data from the CheMin instrument [*Treiman et al.*, 2016; *Le Deit et al.*, 2016]. All Kimberley rocks also show elevated Fe (Table 1), and in the Windjana target both Mg and K are significantly enriched relative to the Sheepbed member [*Le Deit et al.*, 2016] (Table 1, *Wiens et al.* [2013]). Trace elements Zn, Ni, Cu, and Br are strongly enriched. As much as ~4000 ppm Zn was observed by the Alpha Particle X-ray Spectrometer (APXS) in

the Windjana drill cuttings (Table 1), which is well above the highest values detected at Yellowknife Bay (~1300 ppm). The APXS analysis on Stephen showed for the first time at Gale crater a detectable amount of Co (~300 ppm). Most importantly, there is only a slight enrichment in Mn content for the broader Kimberley region compared to average martian crustal values (~0.4 wt% MnO) [*Taylor and McLennan*, 2009], with average local values ~0.5 wt% MnO.

3. High manganese observations

Of the 27 targets analyzed in the Dillinger member, three rock targets have Mn concentrations substantially elevated above the average martian crust and other rocks of the Dillinger member: Stephen (sols 611, 619, 630), Neil (sol 619), and Mondooma (sol 625) (Fig. 2, Table 1). All of these targets sample the resistant mineralized fractures (veins) that crosscut this member. Stephen and Neil are adjacent and expose the flat core of a low-angle fracture fill that weathers in raised relief above the main sandstone outcrop surface, while Mondooma is a similar fin-like feature located in the same bedrock unit a few meters away. ChemCam analyses removed surface dust to reveal dark, specularly reflective surfaces on Stephen and Neil in Mastcam and ChemCam RMI images (Fig. 1e, Fig. 2a, 2b); the surface of Mondooma also appeared significantly darker beneath the dust layer (Fig. 2c). The dust-cleared surfaces of all three targets also exhibit shallow, smaller-scale polygonal fracture patterns spaced by several mm to cm within the larger vein structure that do not appear to be mineralized, e.g., the fracture fill itself has subsequently become fractured (Fig. 2c, 2d).

Point elemental abundances for Stephen were obtained by ChemCam laser-induced breakdown spectroscopy (LIBS) in 17 different locations, with 30 shots (9 locations) and 150 shots (8 locations) obtained in each location for a total of 1470 shot analyses (Fig. 2a). Bulk chemical abundances for Stephen were obtained by 1 overnight APXS integration and a 4-point raster with short 15 minute integrations for a total of 5 analyses (Fig. 2d). Additionally, ChemCam obtained data on both Mondooma and Neil, obtaining 10 sampling locations on each target with 30 shots each for a total of 300 spectra per target (Fig. 2b, 2c).

ChemCam manganese abundances at Stephen, Neil, and Mondooma show shot-averaged MnO abundances of 4.4 wt% (Stephen), 5.5 wt% (Neil), and 6.0 wt% (Mondooma, locations 1-3 on fracture fill surface only) (Table 1) (Text S1). The APXS measurements on Stephen show an average MnO abundance of 3.7 wt%, which is the highest Mn abundance observed by this instrument in Gale crater to date. Because APXS integrates composition over depth, the results from APXS and ChemCam are consistent with one another [*Lanza et al.*, 2014]. Average Mn values from both instruments are well above typical martian igneous values of ~0.4 wt% MnO [*Taylor and McLennan*, 2009].

ChemCam data for Stephen, Neil, and Mondooma display trends in Mn abundance with depth (Fig. 3c, 3d). A compositional depth profile can be measured using multiple laser pulses on a single location. Ablation rates vary by target properties such as mineralogy and hardness but have been measured at ~0.3 µm/pulse in basalt [*Lanza et al.*, 2015]. The first few shots (~1-5) typically contain dust, which is subsequently removed from the rock surface [*Lasue et al.*, 2014]. In locations containing high Mn (Fig. 3a), the Mn abundance was greatest in the first post-dust shots and systematically decreased with succeeding shots (i.e., depth) (Fig. 3c, 3d), with maximum near-surface MnO values of 31.1 wt% (Stephen), 20.3

wt% (Neil), and 34.6 wt% (Mondooma) (Table S2). This pattern implies a compositionally stratified "cement stratigraphy" containing the high Mn phase on what was originally the fracture edge [*Lanza et al.,* 2015]. This interpretation is further supported by MAHLI images of Stephen that show material within the LIBS ablation pits that is brighter than the rock surface (Fig. 3b). MAHLI images of Stephen's surface also confirm the patchy nature of the dark material, captured ChemCam Mn abundance maps (Fig. 3a, b). Although initially it was thought that the high Mn phases on these fin-shaped features could be surface coatings that developed as part of the modern chemical weathering profile, we do not favor this interpretation because the Mn mineralization is limited to fractures that crosscut sedimentary lamination at low angles and is not evenly draped across the topography. Overall, these results support the hypothesis that the Stephen fracture fill is a thin layer that contains elevated Mn, deposited within fractures in the Windjana outcrop material containing average crustal Mn abundances. Such compositional zonation is typical of fracture-filling deposits on Earth, and results in changes in fluid composition over the history of cementation and porosity occlusion [*Grover,* 1983].

The three Mn-rich targets are visibly dark beneath their respective dust layers. Visible to near-infrared reflectance observations from Mastcam [*Hardgrove et al.*, 2015] and ChemCam [*Johnson et al.,* 2015] reveal that Stephen has the lowest reflectance values of any Kimberley target except the Windjana drill cuttings, which are spectrally similar to Stephen at most wavelengths (Fig. 4c). Maximum reflectance values at Stephen are < 0.15, compared to the reflectance maximum of ~0.25 for typical dust-covered soils on Mars [*Lichtenberg et al.,* 2007]. The generally flat spectral profiles and low reflectance values are consistent with laboratory spectra of Mn-oxide minerals (Fig. 4c) [*Fox et al.,* 2015; *Hardgrove et al.,* 2015], which are typically dark in color [*Post,* 1999].

In addition to the targets' dark appearances, geochemical trends also offer insights into the identity of the Mn-rich phase. In ChemCam single-shot data, Si and Ca are inversely correlated with Mn (Fig. S2), suggesting that the high Mn phase is not a silicate and does not contain abundant Ca. ChemCam did not detect Cl or S in the three high Mn targets, both of which are plausible anion pairs for Mn; this along with the absence of C above atmospheric levels in ChemCam data also indicate that the Mn is not present as a sulfate, chloride, or carbonate phase. The APXS composition of Stephen is generally similar to Windjana except for elevated abundances in Mg, Cl, Ni, Cu, Co, and Zn in addition to elevated Mn (Fig. 4a, 4b); however, of the elements showing enrichment, only Ni and Cu show a strong correlation with Mn (Fig. 4b). ChemCam detected elevated Zn in Mondooma, which also contained the highest abundance of Mn, and Neil (Table 1) [*Lasue et al.*, 2016]. Zinc peaks were observable but not quantified in Stephen and Windjana because they are below the limits of detection. Manganese oxides are well known to have an affinity for certain trace metals, in particular Co, Ba, and Ni and to a lesser extent Zn and Cu [*Manceau et al.*, 2007]. The observed mineralogy of the Dillinger member is inconsistent with the strongly oxidizing environment indicated by the high concentrations of Mn, suggesting that the source of Mn is not the surrounding bedrock. In particular, the observation by CheMin X-ray diffraction of abundant magnetite (containing a mixture of Fe(II) and Fe(III) oxidation states) suggest that oxidation of the sediment matrix was limited [*Treiman et al.*, 2016]. It should be noted that CheMin cannot analyze a thin surface layer due to the constraints of the rover drill and sampling mechanism. Only material deeper than ~1.5 cm within the drill hole is delivered to the CheMin instrument [*Anderson et al.*, 2012]; thus the mineralogy of the high Mn materials present in the targets Stephen, Neil, and Mondooma could not be directly measured.

However, given the high abundance of Mn coupled with the appearance and high abundance of numerous trace metals, the observations imply the presence of a Mn-oxide phase. Because Mn-oxides require strong oxidants and sufficient liquid water at typically higher pH ranges to form, their presence in the Dillinger member suggests that its fracture network hosted strongly oxidizing groundwaters at some time in the past.

4. Morphological constraints on timing and origin

The appearance of Mn-oxides in the Dillinger fracture network provides important context for understanding the nature of high Mn concentrations in the Kimberley region. Previous work noted high Mn abundances episodically throughout Curiosity's traverse, but the geologic context was not well constrained [*Lanza et al.*, 2014]. At Kimberley, Mn-oxides have been found only within exposed fracture-filling materials, implying that it is more likely a feature of its lithification and diagenetic history rather than a more recent surface phenomenon, e.g., a rock coating.

The appearance of fracture fills in the Dillinger member provides a bracket for the timing of Mn mineralization. After the Dillinger member sediments were buried and lithified, they were then fractured to create porous networks with a broadly planar geometry. Such fracture networks are extremely common in sedimentary rocks on Earth and could be due to many processes, including fluid advection and hydrofracturing [*Bons et al.*, 2012]. It is not possible to constrain the processes that caused fracture formation and fluid flow in Dillinger other than to note that the deformation stress field must have been oriented such that fracture formation was subhorizontal, implying vertical extension. The absence of elevated Mn or significant alteration in the Dillinger sandstone suggests that the rock was likely cemented prior to fracturing and fluid flow. Our observations are consistent with a system that is rock-buffered

outside of through-going fractures in which Mn is emplaced. On Earth, the chemistry and mineralogy of fracture fills are frequently observed to be unrelated to those of the host rock [*Cox et al.,* 1986]. Thus we infer that Mn was likely concentrated prior to being transported in subsurface fluids to the Kimberley rather than being derived locally from in situ rock weathering.

5. Implications for the early martian environments

The presence of Mn-oxides has important implications for the past redox conditions of Gale groundwater and the martian atmosphere. Precipitation of Mn oxides from fluids moving through the fracture network observed at Kimberley requires highly oxidizing conditions in the groundwater. Very high potential redox reactions are needed to potentially oxidize Mn^{2+} at circumneutral pH (>>500 mV), which requires either O_2 or species derived from O_2 (e.g., reactive oxygen species). The subsurface geological setting of the fractures rules out photooxidation as a mechanism for oxidation; even given a relatively long exposure time at the surface after exhumation, the high concentration of Mn present in these fractures indicates an oxidizing environment at the time of their deposition. Oxychlorine species have been detected by the Sample Analysis at Mars (SAM) instrument in solid samples throughout the rover's traverse [*Glavin et al.,* 2013; *Leshin et al.,* 2013; *Ming et al.,* 2014], some of which can have high enough redox potentials to oxidize Mn(II) [*Sellers et al.,* 2007]. However, none of these oxychlorine detections were associated with Mn enrichments, despite thorough analysis by the CheMin, APXS, and ChemCam instruments [*McLennan et al.,* 2014; *Blake et al.,* 2013; *Vaniman et al.,* 2014; *Blaney et al.,* 2014; *Treiman et al.,* 2016]. Accordingly, we hypothesize that O_2 (or species derived thereby) provides the most reasonable pathway to Mn oxidation and enrichment.

On Earth, O_2 is present in groundwaters due to interaction and equilibrium with the atmosphere, although O_2 can subsequently become depleted along a given fluid flow path due to oxidation of reduced mineral phases and organic matter in the aquifer [*Drever,* 1997]. Groundwaters in basaltic aquifers typically become reducing due to elevated Fe(II) [*Hurowitz et al.*, 2010], which can only be overcome by a very oxidizing fluid system. Consequently, our results suggest that the fluids moving along these fractures were in at least partial contact with the atmosphere and that the atmosphere contained sufficient amounts of O_2 to oxidize Mn. Although thermodynamically favorable above pH ~9, oxidation of Mn(II) by O_2 is kinetically limited without the presence of catalysts, in particular organics and/or microorganisms [*Luther,* 2010; *Learman et al.,* 2011; *Nico et al.,* 2002]. On Mars, where organics are not abundant [*Freissinet et al.,* 2015], the supply and abundance of oxygen and water are the most important factors controlling Mn oxidation. Today Mars has little to no liquid water on its surface and an atmospheric oxygen abundance that is ~10^{-5} times less than the present atmospheric levels on Earth [*Mahaffy et al.,* 2013], which is equivalent to oxygen concentrations on the early Earth [*Pavlov and Kasting,* 2002] prior to large-scale Mn deposition [*Maynard,* 2010]. For Mn to precipitate in martian environments, either concentrations of martian atmospheric O_2 were much higher in the past than observed today or the timescale for water flowing through these fractures were remarkably long. Both possibilities offer interesting perspectives on habitability. However, oxidation in a long timescale, low O_2 aqueous environment is a less favorable explanation because chemical weathering in this environment is expected to remove O_2 from fluids, making them more reducing over time. On Earth, widespread manganese oxidation did not occur prior to the development of an oxygenated atmosphere, despite the presence and long duration of abundant liquid water [e.g., *Hazen et al.*, 2008]. Our results are complimented by the discovery of Mn-oxides at the rim of Endeavor crater in Meridiani Planum by the

Opportunity rover, which also appear as high-Mn fracture fills in a low-Mn host rock [*Arvidson et al.,* 2016]. The appearance of Mn-oxides at a site 1000s of kilometers distant from Curiosity's landing site suggests that the conditions required to concentrate and deposit Mn were present well beyond Gale crater.

These results suggest that the evolution of the martian atmosphere may have been more complex than previously thought. The early martian atmosphere and environment has long been presumed to be reducing [e.g., *Catling and Moore*, 2003], with a gradual progression toward the more oxidizing conditions observed today [e.g., *Dehouck et al.,* 2016]. However, the hypothesis that the martian atmosphere once contained a higher abundance of free oxygen is supported by isotopic evidence from martian meteorites for the presence of ozone in the early martian atmosphere resulting in photolysis in the upper atmosphere [*Farquhar et al.,* 1998], a phenomenon that is observed to a lesser extent today [*Montmessin and Lefèvre,* 2013]. Compositional differences between ancient martian surface rocks and the younger SNC family of martian meteorites also point to oxidation of the mantle early in Mars' history [*Tuff et al.,* 2013]. Gale crater is a Late Noachian/Early Hesperian age feature [*Le Deit et al.,* 2013], with younger sedimentary deposits within the crater and high-Mn fractures that are younger than both the crater and the sediments. Thus the period during which the high-Mn fracture fills were emplaced does not represent the very earliest history of Mars but rather some middle period in which redox conditions were significantly different (and more oxidizing) than in the present day. On Earth, Mn oxidation did not occur until after the evolution of photosynthesis and subsequent rise of O_2 in Earth's atmosphere; enrichment of martian atmospheric O_2 in a similar manner is not an expected interpretation. We note that a range of water-oxygen conditions sufficient for Mn oxidation have O_2 concentrations that are sufficient for aerobic respiration of microorganisms [*Morris and Schmidt,* 2013]; thus on

Mars, high Mn concentrations may be pointing to a past environment that was aerobic, unlike that of early Earth. From the perspective of comparative planetary evolution, this suggests that multiple paths may be important for producing O_2 on terrestrial planets [*Lu et al.,* 2014].

Acknowledgments and Data

We gratefully acknowledge the very helpful comments of M. Osterloo and N. Tosca. This research was carried out in the U.S. under contract from NASA's Mars Program Office. Work in France was carried out with funding from the Centre National d'Etude Spatiale (CNES) and in Canada by the Canadian Space Agency (CSA). This team acknowledges the Jet Propulsion Laboratory (JPL) for developing and leading the Mars Science Laboratory (MSL) Curiosity rover mission. The data reported in this paper are archived at the Planetary Data System, accessible at http://pds-geosciences.wustl.edu/missions/msl/index.htm. Additional data are available as supplementary materials online.

References

Anderson, R.C. et al. (2012), Collecting samples in Gale crater, Mars; an overview of the Mars Science Laboratory sample acquisition, sample processing and handling system, Space Sci. Rev. 170, 57-75.

Arvidson, R.E. et al. (2016), High concentrations of manganese and sulfur in deposits on Murray Ridge, Endeavour Crater, Mars. Am. Mineral. 101, 1389-1405.

Blake, D.F. et al. (2013), Curiosity at Gale crater, Mars: Characterization and analysis of the Rocknest sand shadow, Science 341 (full text online only), doi:10.1126/science.1239505.

Blaney, D.L. et al. (2014), Chemistry and texture of the rocks at "Rocknest", Gale crater: Evidence for iron-rich cements, J. Geophys. Res. Planets 119 (9), 2109-2131.

Bons, P.D., M. A. Elburg, and E. Gomez-Rivas (2012), A review of the formation of tectonic veins and their microstructures, J. Struct. Geol. 43, 33-62.

Cox, S.F., Etheridge, M.A., and Wall, V.J. (1986), The role of fluids in syntectonic mass transport, and the localization of metamorphic vein-type ore deposits. Ore Geol. Rev. 2, 65-86.

Drever, J.I. (1997), The Geochemistry of Natural Waters: Surface and Groundwater Environments, 3rd edition. Prentice Hall, 436 p.

Fabre, C. et al. (2014), In situ prediction of Martian rock and soil compositions using univariate analyses based on the onboard ChemCam calibration targets, Spectrochim. Acta B 99, 34-51.

Farquhar, J., M.H. Thiemens, and T. Jackson (1998), Atmosphere-surface interactions on Mars: delta 17O measurements of carbonate from ALH 84001, Science 280, 1580-1582.

Fox, V. et al. (2015), Characterization of synthetic and natural manganese oxides as Martian analogues, Proc. 46th Lunar and Planetary Sci. Conf., 16-20 March, Houston, TX, abstract no. 2132.

Freissinet, C. et al. (2015), Organic molecules in the Sheepbed Mudstone, Gale Crater, Mars, J. Geophys. Res. Planets 120 (3), 495-514.

Glavin, D.P. et al. (2013), Evidence for perchlorates and the origin of chlorinated hydrocarbons detected by SAM at the Rocknest aeolian deposit in Gale crater, J. Geophys. Res. Planets 118, 1955-1973.

Grotzinger, J.P. et al. (2015), Deposition, exhumation, and paleoclimate of an ancient lake deposit, Gale crater, Mars. Science 350 (6257), aac7575-1-12, doi:10.1126/science.aac7575.

Grover, G. Jr. and J.F. Read (1983), Paleoaquifer and deep burial related cements defined by regional cathodoluminescent patterns, Middle Ordivician Carbonates, Virginia, Am. Assn. Petrol. Geol. Bull. 67 (8), 1275-1303.

Hardgrove, C. et al. (2015), Detecting high manganese phases in Curiosity Mastcam multispectral images and ChemCam passive visible to near infrared spectra, Proc. 46th Lunar and Planetary Sci. Conf., 16-20 March, Houston, TX, abstract no. 2748.

Hazen, R.M. et al. (2008), Mineral evolution, American Mineralogist 93, 1693-1720.

Hurowitz, J.A. et al. (2010), Origin of acidic surface waters and the evolution of atmospheric chemistry on early Mars, Nat. Geosci. 3, 323-326.

Johnson, J.E. et al. (2013), Manganese-oxidizing photosynthesis before the rise of cyanobacteria, Proc. Natl. Acad. Sci. 110 (28), 11238-11243.

Johnson, J.E. et al. (2016), Manganese mineralogy and diagenesis in the sedimentary rock record, Geochim. Cosmochim. Act. 173, 210-231.

Johnson, J.R. et al. (2015), ChemCam passive reflectance spectroscopy of surface materials at the Curiosity landing site, Mars, Icarus 249, 74-92.

Kirschvink, J.L. et al. (2000), Paleoproterozoic snowball Earth: Extreme climatic and geochemical global change and its biological consequences, Proc. Natl. Acad. Sci. 97 (4), 1400-1405.

Lanza, N.L. et al. (2014), High manganese concentrations in rocks at Gale crater, Mars, Geophys. Res. Lett. 41 (16), 5755-5763.

Lanza, N. et al. (2015), Understanding the signature of rock coatings in laser-induced breakdown spectroscopy data, Icarus 249, 62-73.

Lasue, J. et al. (2014), ChemCam analysis of martian fine dust, Proc. 45th Lunar and Planetary Sci. Conf., 17-21 March, Houston, TX, abstract no. 1224.

Lasue, J. et al. (2016), Observations of >5 wt % zinc at the Kimberley outcrop, Gale crater, Mars. J. Geophys. Res. Planets 121, doi:10.1002/2015JE004946.

Learman, D.R. et al. (2011), Coupled biotic-abiotic Mn(II) oxidation pathway mediates the formation and structural evolution of biogenic Mn oxides, Geochim. Cosmochim. Acta 75, 6048-6063.

Le Deit, L. et al. (2013), Sequence of infilling events in Gale Crater, Mars: Results from morphology, stratigraphy, and mineralogy. J. Geophys. Res. Planets 118, 2439-2473.

Le Deit, L. et al. (2016), The potassic sedimentary rocks in Gale crater, Mars, as seen by ChemCam onboard Curiosity, Proc. 47th Lunar and Planetary Sci. Conf., 21-25 March, Houston, TX, abstract no. 1163.

Leshin, L.A. et al. (2013), Volatile, isotope, and organic analysis of Martian fines with the Mars Curiosity rover, Science 341 (full text available online only), doi:10.1126/science.1238937.

Lichtenberg, K. A. et al. (2007), Coordinated analyses of orbital and Spirit rover data to characterize surface materials on the cratered plains of Gusev crater, Mars, J. Geophys. Res. 112 (E12S90), doi:10.1029/2006JE002850.

Lu, Z. et al. (2014), Evidence for direct molecular oxygen production in CO2 photodissociation, Science 3 (346) 61-64.

Luther, G.W. III. (2010), The role of one- and two-electron transfer reactions in forming thermodynamically unstable intermediates as barriers in multi-electron redox reactions, Aquat. Geochem. 16, 395-420.

Mahaffy, P.R. et al. (2013), Abundance and isotopic composition of gases in the Martian atmosphere from the Curiosity rover, Science 341 (6143), 263-266.

Manceau, A. et al. (2007), Natural speciation of Ni, Zn, Ba, and As, in ferromanganese coatings on quartz using X-ray fluorescence, absorption, and diffraction, Geochim. Cosmochim. Acta 71, 95-128.

Maynard, J.B. (2010), The chemistry of manganese ores through time: A signal of increasing diversity of Earth-surface environments, Economic Geology 105, 535-552.

McLennan S.M. et al. (2014), Elemental geochemistry of sedimentary rocks in Yellowknife Bay, Gale crater, Mars, Science 343 (full text online only), doi:10.1126/science.1244734.

Ming, D.W. et al. (2014), Volatile and organic compositions of sedimentary rocks in Yellowknife Bay, Gale crater, Mars, Science 343 (full text online only), doi:10.1126/science.1245267.

Montmessin, F. and F. Lefèvre (2013), Transport-driven formation of a polar ozone layer on Mars, Nat. Geosci. 6, 930-933.

Morris, R.L. and T.M. Schmidt (2013), Shallow breathing: bacterial life at low O2, Nat. Rev. Microbiol. 11, 205-212.

Nico, P.S., C. Anastasio, and R.J. Zasoski (2002), Rapid photo-oxidation of Mn(II) mediated by humic substances, Geochim. Cosmochim. Acta 66 (23), 4047-4056.

Ollila, A.M. et al. (2014), Trace element geochemistry (Li, Ba, Sr, and Rb) using Curiosity's ChemCam: Early results for Gale crater from Bradbury Landing Site to Rocknest, J. Geophys. Res. Planets 119, 255-285.

Pavlov, A.A. and J.F. Kasting (2002), Mass-independent fractionation of sulfur isotopes in Archean sediments, Astrobiol. 2 (1), 27-41.

Post, J.E. (1999), Manganese oxide minerals: Crystal structures and economic and environmental significance, Proc. Natl. Acad. Sci. 96, 3447-3454.

Sellers, K. et al. (2007), Perchlorate: Environmental Problems and Solutions, 1st ed., 226 pp., CRC Press, Boca Raton, FL.

Taylor, S.R. and S.M. McLennan (2009), Planetary Crusts: Their Composition, Origin, and Evolution. Cambridge University Press: New York, 378 p.

Treiman, A.H. et al. (2016), Mineralogy, provenance, and diagenesis of a potassic basaltic sandstone on Mars: CheMin X-ray diffraction of the Windjana sample (Kimberley area, Gale Crater), J. Geophys. Res. Planets 21, 75-106.

Tuff, J., Wade, J., and Wood, B.J. (2013), Volcanism on Mars controlled by early oxidation of the upper mantle. Nature 498, 342-345.

Vaniman, D.T. et al. (2014), Mineralogy of a mudstone at Yellowknife Bay, Gale crater, Mars, Science 343, doi: 10.1126/science.1243480.

Wiens, R.C. et al. (2013), Pre-flight calibration and initial data processing for the ChemCam laser-induced breakdown spectroscopy instrument on the Mars Science Laboratory rover, Spectrochim. Acta B 82, 1-27.

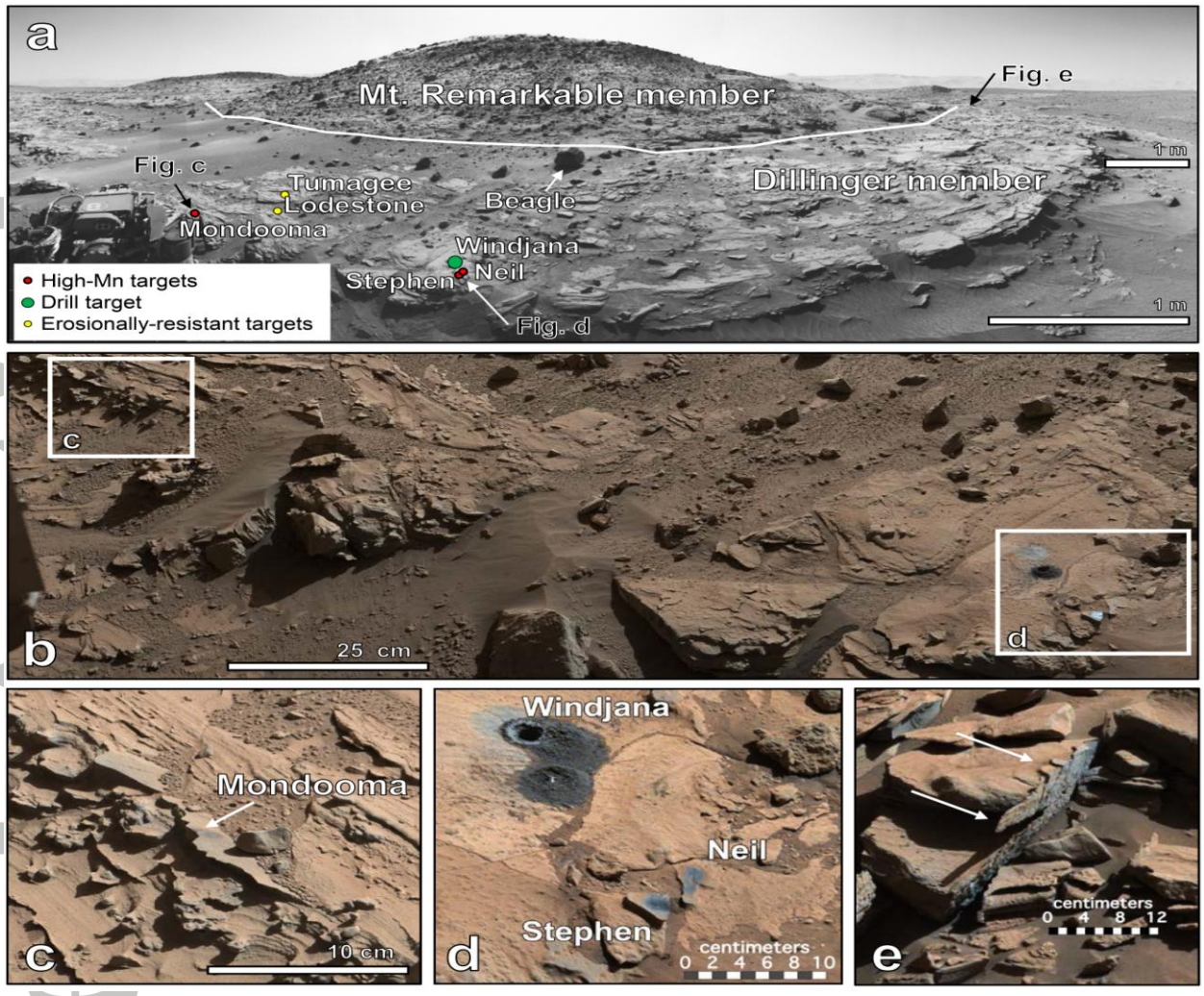

Figure 1. (a) Upper members of the Kimberley formation; the white line indicates the inferred contact between the Mt. Remarkable and Dillinger members. North is to the right. (Navcam-Left cylindrical projection mosaic N_L000_0621XEDR031CYLTSB1330). **(b)** A closer view of the Dillinger member; high Mn target Mondooma is located within the white box labeled **c**, while high Mn targets Stephen and Neil are seen within the white box labeled **d** along with the drill hole at target Windjana (mosaic of Mastcam-Right images from sequence mcam02600, sol 617). **(c)** High Mn target Mondooma, which is a resistant fin-like feature that emerges from within the outcrop; high Mn was only observed on the top of the fin (first three sampling locations, see Fig. 2c for details) (Mastcam-Right image 0626MR0026790000401609E01). **(d)** High-Mn targets Stephen and Neil in relation to the Windjana drill hole (Mastcam-Right image 0626ML0026760010302385E01). **(e)** White arrows indicate an example of resistant material that potentially fills orthogonal fractures (Mastcam-Left image 0597ML0025180010301188E01).

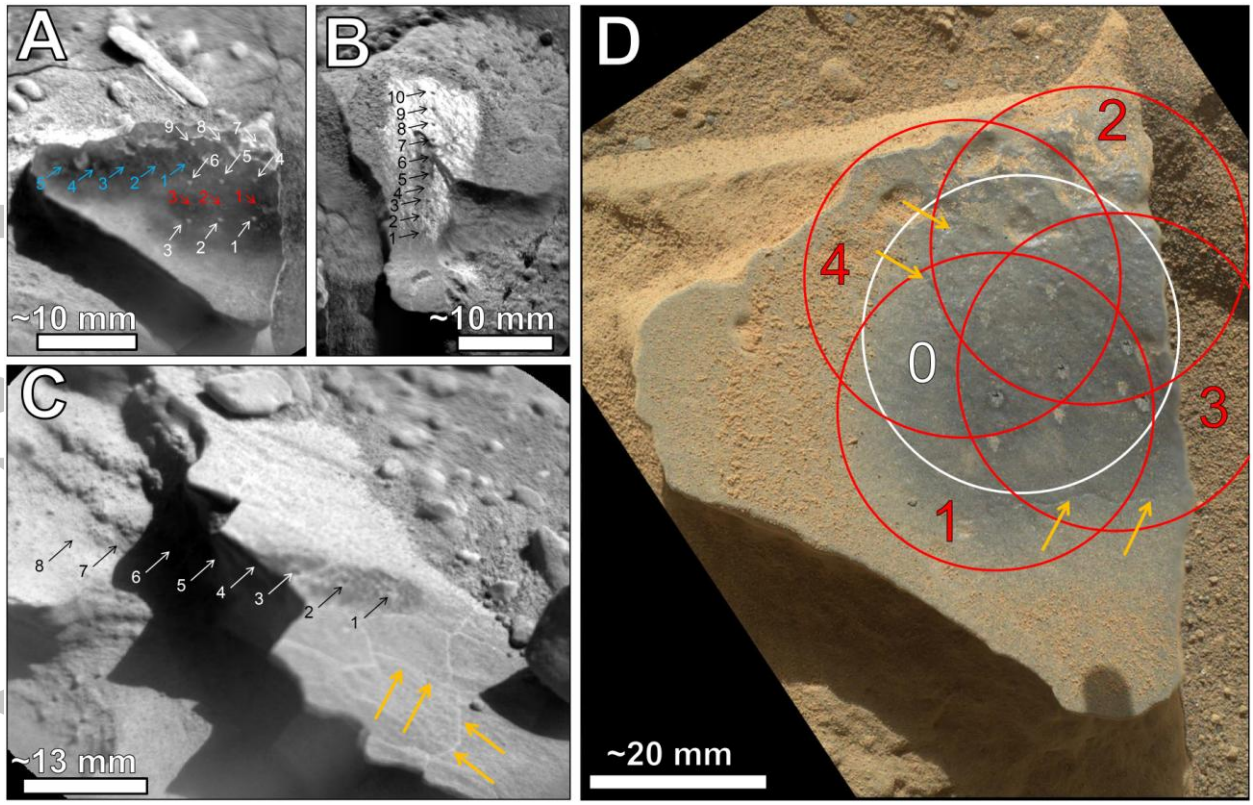

Figure 2. Kimberley targets containing high manganese. **(a)** ChemCam remote micro-imager (RMI) image of high-Mn target Stephen with ChemCam LIBS analysis locations marked: Sol 611 3x3 raster with 30 shots/location (white, ccam01611), sol 619 1x3 raster with 150 shots/location (red, ccam03619), and sol 630 1x5 raster with 150 shots/location (blue, ccam01630). **(b)** RMI image of high-Mn target Neil with LIBS analysis locations marked (ccam04619). **(c)** RMI image mosaic of high-Mn target Mondooma with LIBS analysis locations 1-8 marked, sol 625 1x10 raster with 30 shots/location; note the fracture pattern on the top of the fin (yellow arrows) (ccam01625). **(d)** MAHLI image of target Stephen showing APXS analysis locations; circle 0 (white) indicates the location of the APXS overnight analysis and circles 1-4 (red) show the locations of the 2x2 APXS raster (MAHLI focus merge product 0627MH0004070000203592R00, 5 cm standoff); note similar surface fractures to those seen on the surface of Mondooma (yellow arrows).

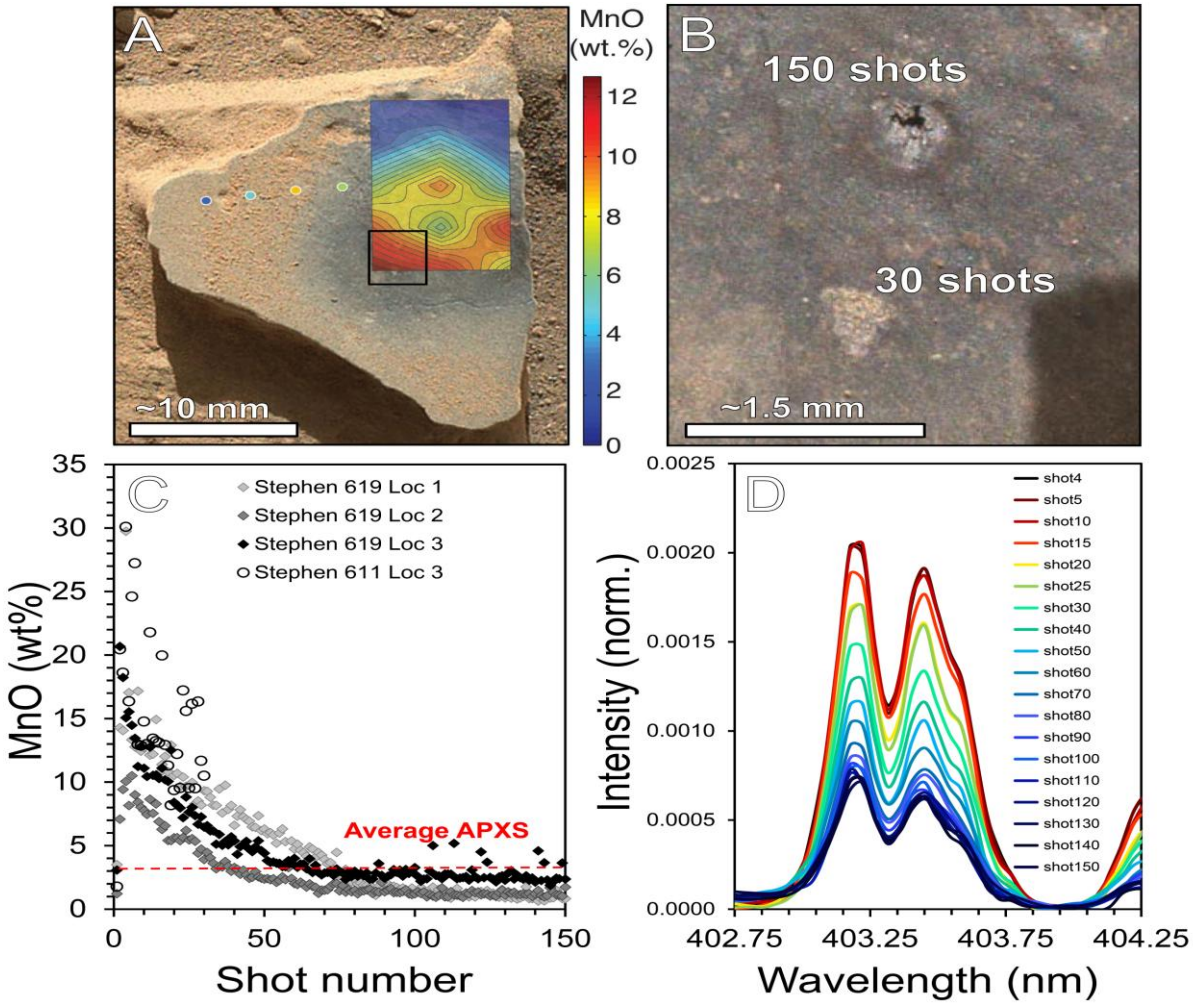

Figure 3. **(a)** Spatial variation in manganese abundance on Stephen. The MAHLI image (0627MH0001900010203555C00) is overlain by a linearly interpolated surface of the median MnO abundance (wt%) from the first 30 LIBS shots from every location in the 3x3 and 1x3 ChemCam analyses; median MnO abundances of the 1x5 raster indicated by points. Location of panel **b** indicated by black box. **(b)** Close up of two LIBS analysis pits visible on Stephen, one of 30 shots (location 3 in the 3x3 raster) and the other of 150 shots (location 3 in the 1x3 raster). Both analyses have removed some dark material to reveal a brighter-toned material beneath (sub-frame of MAHLI 0627MH0004070000203588R00, 1 cm standoff). **(c)** Manganese abundance by shot (depth) for all three locations in the Stephen 1x3 and location 3 of the 3x3 raster (shown in panel **b**). After 1-2 shots containing dust, Mn abundance is high in the early shots and systematically decreases as the laser penetrates deeper into the rock's surface. **(d)** Shot-to-shot LIBS spectral peak intensities for the main Mn doublet region (~402.75-403.75 nm) for location 3 of the Stephen 1x3 150-shot raster shown in panels **b** and **c**. Spectra color indicates MnO abundance (wt%) in the same scale as shown in panel **a** with some modification to indicate individual shots.

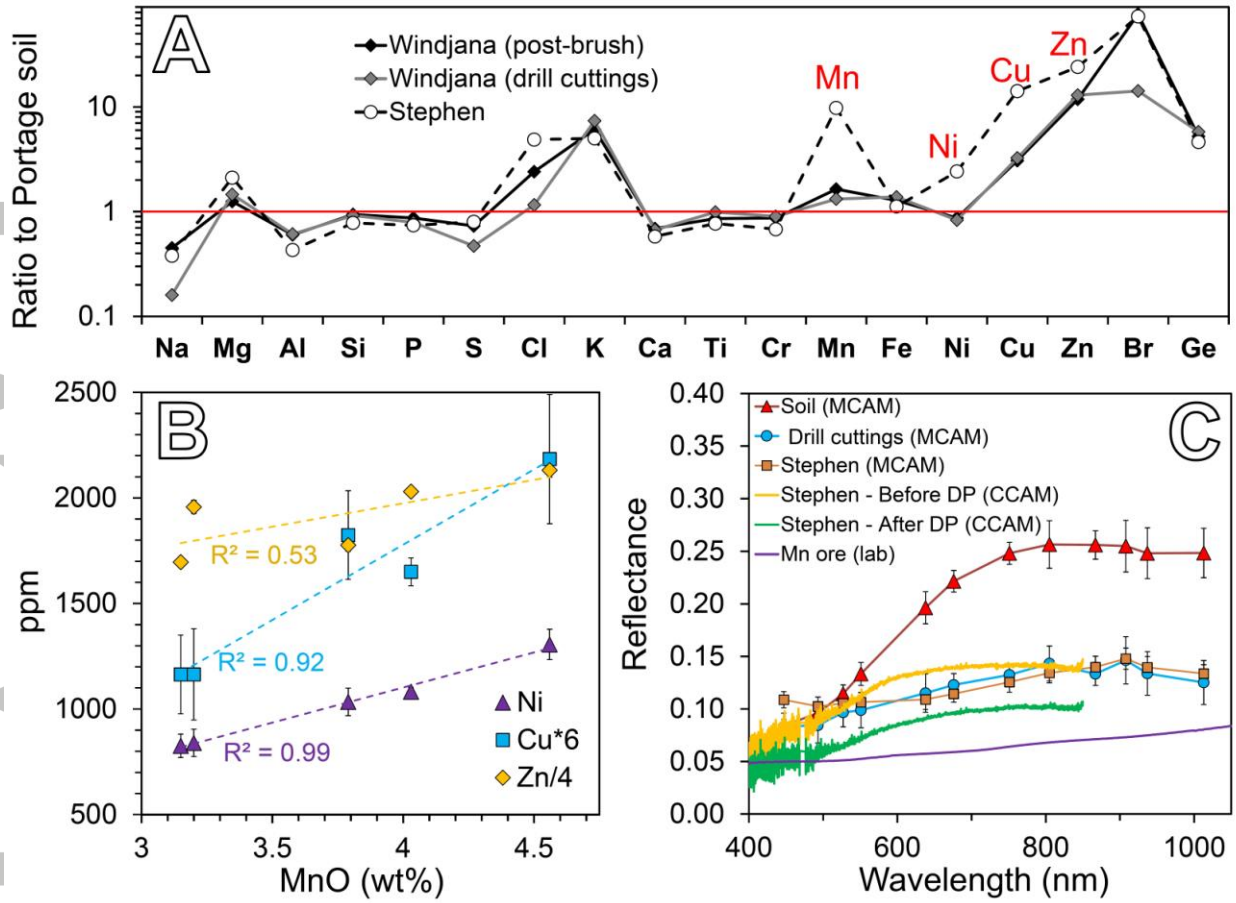

Fig. 4. (a) APXS elemental compositions ratioed to the soil Portage (sol 89) for the brushed Windjana target (sol 612), Windjana drill cuttings (sol 623), and Stephen (sol 627), after first two ChemCam analyses. **(b)** Relationship between measured MnO (wt%) and Ni, Cu, and Zn (ppm); Cu values have been multiplied by 6 and Zn values have been divided by 4 for clarity, and error bars represent 2-sigma standard deviation (note that error bars for Zn are smaller than plot symbols and range ~12-33 ppm). There is a strong correlation between MnO and Ni and Cu, while Zn does not appear to be strongly correlated with MnO. **(c)** Reflectance spectra of Stephen from the sol 626 Mastcam multispectral observation compared to sol 630 ChemCam passive reflectance spectra acquired at the first depth profile location on target Stephen before and after 150 laser shots. Error bars on each Mastcam spectrum represent 1-sigma standard deviation of averages. Mastcam spectra of the Windjana drill cuttings and undisturbed soil and a laboratory Mn-oxide-rich ore (NCS-DC28044, see Table S1) are shown for comparison.

Table 1. Major element compositions of high Mn targets and regional bedrock from ChemCam and APXS in wt% for oxides and Cl, ppm for others. nd = not detected, nq = not quantified. Number of analysis locations included is indicated in parentheses. ChemCam abundances represent averages of 25 shots per location after the first five shots, which are removed to exclude dust. For single-shot major element compositions and Mn abundances, see Table S2.

Instrument	*APXS*	CCAM	CCAM	CCAM	*APXS*	*APXS*	CCAM
Sample	*Stephen (5)*	Stephen (17)	Neil (10)	Mondooma (3)	*Windjana post-brush (1)*	*Windjana drill cuttings (3)*	Windjana (25)
SiO2SiO2	*34*	41.2	40.4	42.9	*40.4*	*39.5*	44.7
TiO2TiO2	*0.9*	0.7	0.8	0.8	*1*	*1.2*	0.9
Al2O3Al2O3	*4.4*	6.6	6.2	7.3	*5.6*	*5.7*	7.4
FeOT	*21.2*	17.0	17.5	17.8	*24.5*	*26.2*	18.0
Cr2O3Cr2O3	*0.3*	nq	nq	nq	*0.4*	*0.4*	nq
MnO	*3.7*	4.4	5.5	6.0	*0.7*	*0.5*	0.5
MgO	*17.9*	12.8	13.4	13.2	*10.9*	*12.8*	9.6
CaO	*4.3*	4.1	3.5	3.5	*5*	*4.9*	4.8
Na2ONa2O	*1.1*	1.8	1.8	2.7	*1.2*	*0.4*	1.3
K2OK2O	*2.4*	1.7	1.5	2.2	*3*	*3.6*	2.9
P2O5P2O5	*0.7*	nd	nd	nd	*0.8*	*0.7*	nd
SO3SO3	*4.6*	nd	nd	nd	*4*	*2.6*	nd
Cl	*3.3*	nd	nd	nd	*1.7*	*0.8*	nd
Ni	*1010*	nd	nd	nd	*390*	*380*	nd
Zn	*7700*	nq	4017	15425	*4000*	*4300*	nq
Cu	*270*	nd	nd	nd	*60*	*40*	nd
Br	*1810*	nd	nd	nd	*1980*	*430*	nd